

A numerical study of the motion of drops in Poiseuille flow. Part 1. Lateral migration of one drop

By SAEED MORTAZAVI¹ AND GRÉTAR TRYGGVASON²

¹Department of Aerospace Engineering, University of Michigan, Ann Arbor, MI 48109, USA

²Department of Mechanical Engineering and Applied Mechanics, University of Michigan,
Ann Arbor, MI 48109, USA

(Received 29 December 1998 and in revised form 14 January 2000)

The cross-stream migration of a deformable drop in two-dimensional Hagen–Poiseuille flow at finite Reynolds numbers is studied numerically. In the limit of a small Reynolds number (< 1), the motion of the drop depends strongly on the ratio of the viscosity of the drop fluid to the viscosity of the suspending fluid. For viscosity ratio 0.125 a drop moves toward the centre of the channel, while for ratio 1.0 it moves away from the centre until halted by wall repulsion. The rate of migration increases with the deformability of the drop. At higher Reynolds numbers (5–50), the drop either moves to an equilibrium lateral position about halfway between the centreline and the wall – according to the so-called Segre–Silberberg effect or it undergoes oscillatory motion. The steady-state position depends only weakly on the various physical parameters of the flow, but the length of the transient oscillations increases as the Reynolds number is raised, or the density of the drop is increased, or the viscosity of the drop is decreased. Once the Reynolds number is high enough, the oscillations appear to persist forever and no steady state is observed. The numerical results are in good agreement with experimental observations, especially for drops that reach a steady-state lateral position. Most of the simulations assume that the flow is two-dimensional. A few simulations of three-dimensional flows for a modest Reynolds number ($Re = 10$), and a small computational domain, confirm the behaviour seen in two dimensions. The equilibrium position of the three-dimensional drop is close to that predicted in the simulations of two-dimensional flow.

1. Introduction

Drops suspended in another fluid in channel flow are encountered in a wide variety of technologically important processes such as liquid–liquid extraction and the flow of oil and water through pipelines (see Schramm 1992; Berkman & Egloff 1941, and Joseph & Renardy 1992). Because the distribution of drops through the cross-section of the channel determines the flow rate, for a given pressure drop, determining the lateral migration of the drops and their final equilibrium position is of particular interest. Several investigators have examined the problem, but most focused on flow at Reynolds number that is either zero or $O(1)$. Here we examine the behaviour over a larger range of Reynolds numbers. These conditions are particularly relevant to flow in micro-gravity, where dispersed flow is observed over a much larger flow rate range than under terrestrial conditions, and the drops can be large.

The review article by Brenner (1966) discusses early experimental studies. The migration of neutrally buoyant solid particles and drops was studied by Goldsmith & Mason (1961, 1962) in tube flow, at near-zero Reynolds number. They did not observe lateral migration for solid spheres moving over 50 000 tube radii. Experiments conducted by Karnis, Goldsmith & Mason (1966*a*) on a suspension of rigid particles at small Reynolds numbers in a tube flow did not show any concentration gradient across the tube cross-section in the range of volume fractions examined either. In contrast to solid particles, highly deformable liquid drops with viscosity ratios ranging from 0.0002 to 4.8 migrate toward the tube axis at a rate that increases with the flow rate and drop size. Nearly spherical drops at low flow rates migrate away from the tube wall, although they do not always reach the tube axis. Similar experiments were conducted by Karnis & Mason (1967) who observed that liquid drops with a small viscosity ratio (0.0002–0.02) migrate toward the tube centre and reach the tube axis at small Reynolds numbers. Hiller & Kowalewski (1987) conducted experiments on a very dilute suspension of droplets in a plane Poiseuille flow in the limit of creeping flow. They found that drops with low viscosity ratios (0.1) eventually concentrate at the channel axis. At high viscosity ratios (1), however, the concentration peak moved to a position between the wall and the centreline. For studies of the motion of large drops in a tube see Couillette & Pozrikidis (1998) and the review article by Olbright (1996).

The effect of inertia on the motion of particles in a Poiseuille flow was studied experimentally by Segre & Silberberg (1962*a, b*) who performed experiments with a dilute suspension of neutrally buoyant solid particles for a wide range of Reynolds numbers and particle sizes. They observed that solid particles migrate away from both the tube axis and the wall, forming a concentrated layer at about half the distance between the axis and the wall. This effect was further investigated by Karnis, Goldsmith & Mason (1963, 1966*a, b*) using spherical particles and drops. They found that deformable drops migrate to the tube axis if their viscosity is low (similar to the creeping flow limit), but behave like solid particles at high viscosity ratios and settle down at a distance halfway between the channel wall and the centreline. Experimental studies of solid spheres in a channel have also been conducted by Oliver (1962), Jeffrey & Pearson (1965), and Tachibana (1973), confirming the results of Segre & Silberberg (1962*a, b*).

Theoretical investigations of the lateral migration of drops in Poiseuille flow have addressed the effects of deformation and inertia separately. Theories for the lateral migration of deformable drops are restricted to the Stokes flow limit. Chan & Leal (1979) examined a nearly spherical drop that is small compared to the channel width, and obtained a closed-form solution for the cross-stream migration velocity in a linear shear flow and in two-dimensional Poiseuille flow assuming that $\lambda < 1/Ca$, where $\lambda = \mu_i/\mu_o$ is the viscosity ratio and Ca is the capillary number. The deformed shape of the drop was predicted as a function of the governing parameters. For values of λ between 0.5 and 10, the drop migrated to the walls, but for $\lambda < 0.5$ and $\lambda > 10$ it moved to the centreline. The predicted axial velocity of the drop always lagged behind the undisturbed flow in Poiseuille flow.

Theoretical studies of the effect of inertia have been limited to spherical particles. Ho & Leal (1974) obtained the equilibrium position and the trajectory of a small, neutrally buoyant sphere in a linear shear flow, as well as in Poiseuille flow, using a regular perturbation expansion for small particle Reynolds number. They derived a closed-form solution for the lateral force and concluded that a neutrally buoyant sphere in Poiseuille flow migrates to an equilibrium position given by $Z_{eq} = 0.2H$, where H is the channel height and Z is the distance from the wall. Their results are in

good agreement with the experimental observations of Segre & Silberberg (1962*a, b*) and Tachibana (1973). Additional analytical studies have been reported by Vasseur & Cox (1976) and Cox & Hsu (1977) who obtained an equilibrium position that was slightly closer to the wall than that predicted by Ho & Leal. Particles close to the wall also had a different migration velocity.

More recently, Schonberg & Hinch (1989) used a singular perturbation method similar to the one used by Saffman (1965) to study the lateral migration of a rigid particle in Poiseuille flow at higher Reynolds numbers, addressing the effect of the Reynolds number. Unlike Cox & Brenner (1968), Ho & Leal (1973), and Vasseur & Cox (1976), they included an outer region where inertial effects are comparable to viscous effects. The particle size, however, was still assumed to be small compared to the channel dimension. Schonberg & Hinch did not observe any change in the equilibrium position of the particle with Reynolds number for $Re_b < 15$, and their results were essentially identical to those of Vasseur & Cox (1976) in this range. However, the equilibrium distance from the wall was found to change from $Z = 0.185H$ at low Reynolds numbers, to $Z = 0.16H$ at a Reynolds number of 75. Agreement with the experimental results of Segre & Silberberg (1962*a, b*) worsens as the Reynolds number is raised. A review on the motion of solid spheres in shear flows was given by Feuillebois (1989).

Recently, the migration of deformable drops in shear flow at zero Reynolds number was studied by numerical simulation using boundary-integral methods. The two-dimensional simulation of a few droplets performed by Zhou & Pozrikidis (1993*a, b*) for Couette flow, and by Zhou & Pozrikidis (1994) for Poiseuille flow, showed that deformable drops migrate away from the walls. Zhou & Pozrikidis (1994) found that drops having the same viscosity as the surrounding fluid migrate toward the centreline of the channel. Simulations of a single drop with a viscosity ratio of 10 showed that if it is initially close to the centreline, it moves to the wall; whereas if it is initially close to the wall, it migrates toward the centreline. This result suggested that deformable drops could move to an equilibrium position at about halfway between the wall and the centreline, for this viscosity ratio. Three-dimensional simulations of a single drop close to a plane wall in simple shear flow done by Kennedy, Pozrikidis & Skalak (1994) also showed that drops always migrate away from the wall for a wide range of viscosity ratios and capillary numbers. Other studies of the motion of a single drop at zero Reynolds number were conducted by Martinez & Udell (1990), and Khayat, Luciani & Utracki (1997), for example. In these papers, however, axial symmetry is assumed, and the drops stay on the centreline at all times. Fully three-dimensional drops in a circular tube were simulated by Couillette & Pozrikidis (1998) using a boundary-integral method and Bozzi *et al.* (1997) have simulated axisymmetric drops at finite Reynolds numbers.

Feng, Hu & Joseph (1994*a, b*) conducted two-dimensional simulations of solid particles in a Poiseuille flow at finite Reynolds numbers using a finite element method with a locally adaptive moving mesh. Their results were in good agreement with the perturbation theory of Ho & Leal (1974) and the experiments of Segre & Silberberg (1962*a, b*), although the equilibrium position predicted by their simulations was closer to the channel axis.

In this paper, the migration of a neutrally buoyant deformable drop at finite Reynolds numbers is studied by numerical simulation. The present study is similar to that by Feng *et al.* (1994*a, b*), except that the particles are deformable, and that a few three-dimensional simulations are included. The dependence of the drop migration on deformation, viscosity ratio, and Reynolds number are examined.

2. Governing equations and dimensionless parameters

The unsteady motion of a Newtonian drop in a Newtonian fluid is governed by the Navier–Stokes equations. A single vector equation can be written for the whole flow field by allowing the density and viscosity to vary discontinuously, and by including surface tension as a generalized body force concentrated at the interface. The ‘one-field’ equation is

$$\frac{\partial \rho \mathbf{u}}{\partial t} + \nabla \cdot (\rho \mathbf{u} \mathbf{u}) = -\nabla p + \nabla \cdot \mu (\nabla \mathbf{u} + \nabla \mathbf{u}^T) - \int \sigma \kappa \mathbf{n} \delta(\mathbf{x} - \mathbf{X}(s, t)) ds. \quad (1)$$

Here, \mathbf{u} , p , ρ , μ and σ are the velocity, pressure, density, viscosity and interfacial tension, respectively; κ is twice the mean curvature for three-dimensional flow, and the curvature for two-dimensional flow; \mathbf{n} is the outward unit normal to the drop surface, and $\mathbf{X}(s, t)$ is a Lagrangian representation of the interface; δ is the two- or three-dimensional delta function; and the line or surface integral is over the interface. The fluids are assumed to be incompressible and immiscible, and the material properties are constant:

$$\frac{D\rho}{Dt} = 0 \quad (2)$$

$$\frac{D\mu}{Dt} = 0. \quad (3)$$

Incompressibility requires a solenoidal velocity field,

$$\nabla \cdot \mathbf{u} = 0. \quad (4)$$

The geometry of the flow domain is shown in figure 1. The computational domain is periodic in the x -direction and bounded by no-slip walls in the z -direction. In three-dimensional flow, the domain is also periodic in the y -direction. The flow through the channel is driven by a constant pressure gradient. In the problem formulation, we write

$$\nabla p = \nabla P_o + \nabla p' \quad (5)$$

where ∇P_o is the externally specified pressure gradient and $\nabla p'$ is the perturbation pressure gradient to be computed as part of the solution. The velocity is initially set equal to the parabolic velocity profile corresponding to the imposed constant pressure gradient if there are no drops in the channel. A drop of undeformed radius a is then placed into the flow without affecting the velocity. Initially, the drop is therefore deformed by the parabolic velocity profile. However, surface tension quickly limits the deformation and the fluid velocity is modified due to the presence of the drop. Since the pressure gradient is specified, the flow rate generally changes as the solution evolves.

In all the simulations presented here, gravity is neglected. Therefore, buoyancy effects are absent, even when the drops are denser than the suspending fluid. The governing non-dimensional numbers are the Reynolds number Re , the Weber number We , the ratio of the viscosity of the drop fluid to the suspending medium $\lambda = \mu_i/\mu_o$, the density ratio $\alpha = \rho_i/\rho_o$, and the ratio of the radius of the undeformed drop to the height of the channel $\zeta = a/H$. The viscosity and density of the drop liquid are denoted by μ_i and ρ_i , respectively, and the suspending fluid has viscosity μ_o and density ρ_o . The channel is a rectangle with height H , in two dimensions, and a rectangular box with a small thickness in three dimensions. Most of the two-dimensional simulations use a square domain. In the literature, the Reynolds number has been defined in various

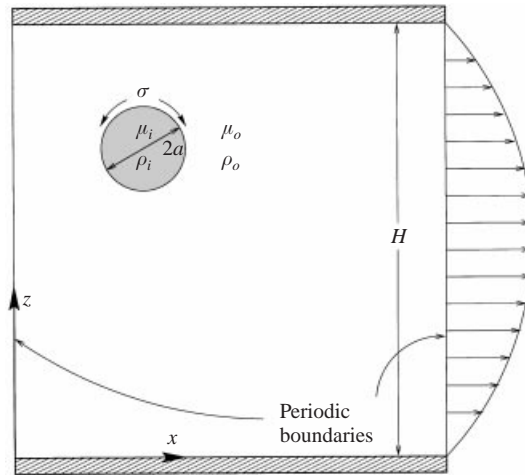


FIGURE 1. The geometry for the simulation of a drop in a rectangular channel. A drop of radius a with density and viscosity ρ_i and μ_i is suspended in a Newtonian fluid with density and viscosity ρ_o and μ_o . A constant pressure gradient drives the flow.

ways, depending on the chosen reference velocity and length. The channel Reynolds number is defined in terms of the undisturbed channel centreline velocity U_c , and the channel height, as $Re_b = \rho_o U_c H / \mu_o$. A characteristic velocity can also be defined based on the average velocity difference across the particle, $U_c a / H$, giving the particle Reynolds number $Re_p = \rho_o U_c a^2 / (\mu_o H)$. A Reynolds number based on the centreline velocity and the drop diameter (d) is defined by $Re_d = \rho_o U_c d / \mu_o$. These Reynolds numbers are related by $Re_p = Re_d (a / (2H))$, and $Re_b = Re_d (H / d)$. A Weber number is defined by the centreline velocity and the drop diameter: $We = \rho_o U_c^2 d / \sigma$. In the small inertia limit where viscous stresses are dominant, the proper non-dimensional number for the interfacial tension is the capillary number, which expresses the ratio of viscous stress to the interfacial tension, $Ca = U_c \mu_o / \sigma$. Bentley & Leal (1986) and Stone & Leal (1989), examined the bursting of drops in a linear shear flow, and defined the capillary number based on the shear velocity $Ca = G a \mu / \sigma$ where G is the shear rate. This results in lower numerical values than used here. Non-dimensional time is defined by $\tau = t U_c / H$.

3. Numerical method

The motion of the drops is simulated using the finite difference/front tracking method developed by Unverdi & Tryggvason (1992*a, b*). The Navier–Stokes equations are solved by a second-order projection method using centred differences on a fixed, staggered grid. To keep the boundary between the drop and the ambient fluid sharp, and to accurately compute the surface tension, the boundary is represented by connected marker points (the ‘front’) that are advected by the flow velocity, interpolated from the fixed grid. If the front is stretched by the flow, the marker points move apart and the front resolution suffers. To maintain the resolution, new marker points are inserted when the distance between points becomes too large. Points are also deleted if the distance becomes smaller than a prescribed value. The singularities at the front (density and viscosity gradients and surface tension) are approximated on the fixed grid by smooth functions with a compact support. The

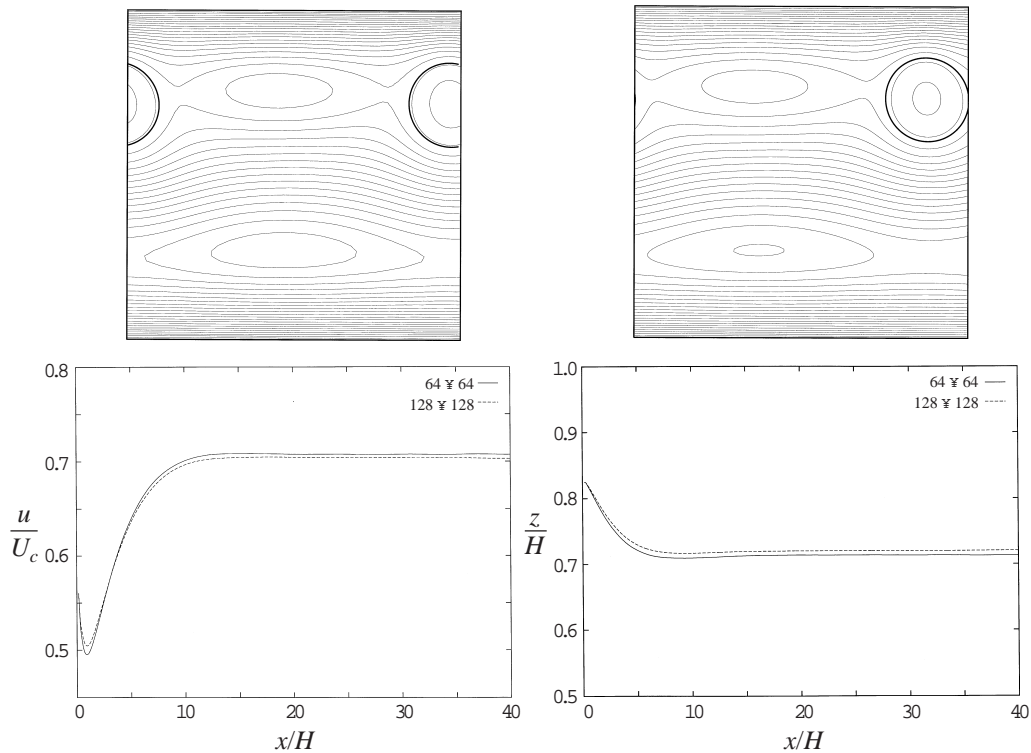


FIGURE 2. Effect of the resolution on the lateral migration of a drop in a plane Poiseuille flow at $Re_d = 10$, $\alpha = \gamma = 8$, $We = 0.5$ and $\zeta = 0.125$. The streamlines are plotted at the top, and the drop axial velocity and lateral position are plotted versus the axial location for two resolutions at the bottom.

density and viscosity fields are reconstructed at each time step by integrating the smooth grid delta function, after the front has been moved, and the body force due to surface tension is added to the nodal values of the discrete Navier–Stokes equations. The elliptic pressure equation is solved by a multigrid method (Adams 1989) when the density of the drop is different from the suspending fluid, and by a fast Poisson solver (FISHPACK) when the densities are equal. For a detailed description of the method and various validation tests, see Unverdi & Tryggvason (1992*a, b*) and Tryggvason *et al.* (1998*a, b*).

4. Results

4.1. Resolution tests

To determine how well the flow field needs to be resolved, and to ensure grid independence of the solution, resolution tests were done for several Reynolds numbers. As expected, we find that as the Reynolds number increases, finer grids are required and the drop needs more time to reach an equilibrium position.

Figure 2 shows the streamlines, the trajectory, and the axial velocity for a two-dimensional drop at Reynolds number $Re_d = 10$ at two different grid resolutions with 64^2 or 128^2 grid points, corresponding to 16 or 32 grid points per drop diameter for the low or high resolution, respectively. The flow parameters are: $We = 0.5$, $\alpha = \lambda = 8$, and $\zeta = 0.125$. The drop is initially released close to the upper wall. The streamlines

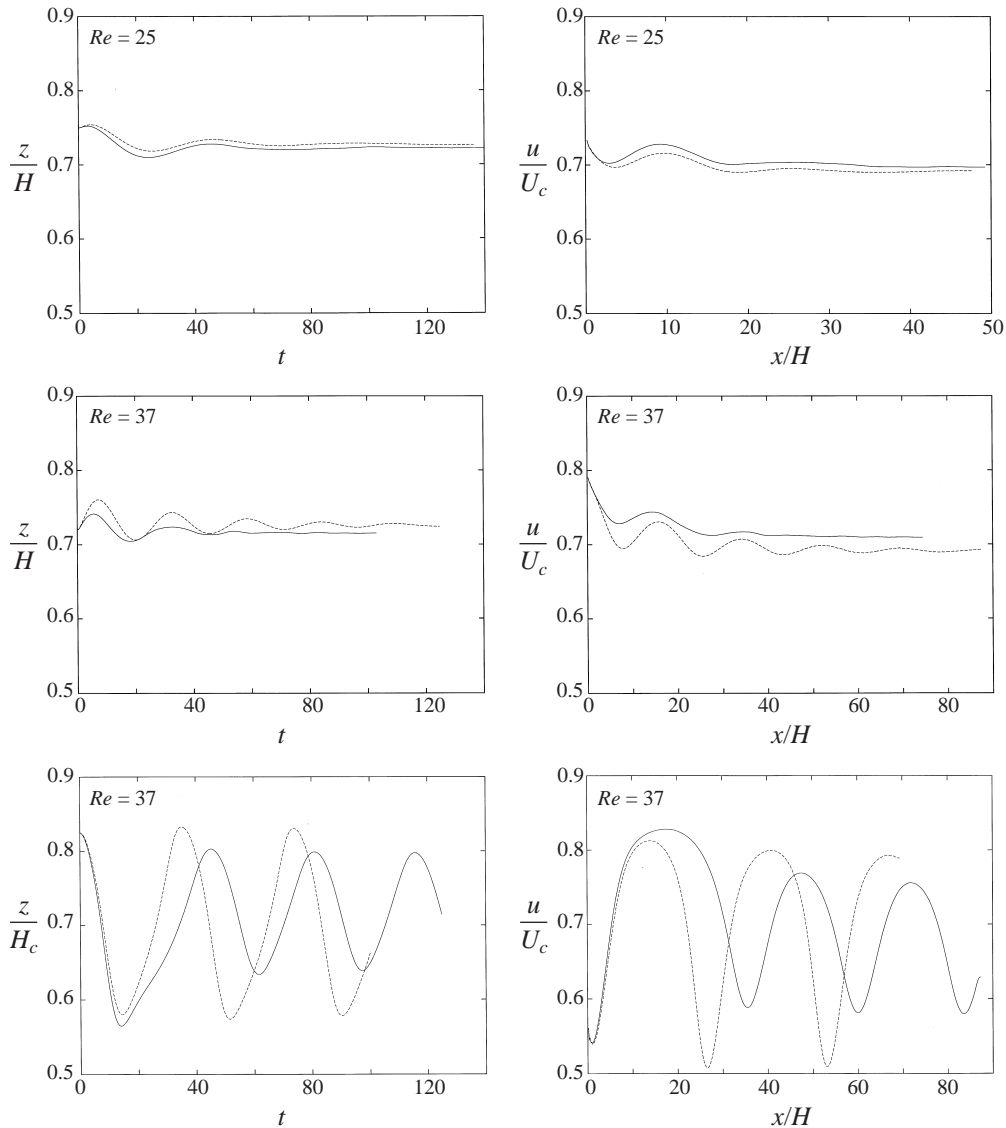


FIGURE 3. Resolution test at different Reynolds numbers. Here, $\gamma = 8$, except for the bottom frames where $\gamma = 2$. The solid and the dotted lines show results at 128×128 and 256×256 grid resolution, respectively. Other flow parameters are: $\alpha = 8$ and $We = 0.5$. The Reynolds number is based on the centreline velocity and the drop diameter.

are shown at the same time for both resolutions, after the drop has reached an equilibrium lateral position. The high-resolution drop moves a little slower than the low-resolution drop, but otherwise the results are in good agreement. The equilibrium positions differ by about 0.6% of the channel height, and the difference between the axial velocities is around 0.4% of the centreline velocity.

Figure 3 presents additional tests at higher Reynolds numbers, and at a different viscosity ratio with grid sizes 128^2 and 256^2 . The latter results in 64 grid points per drop diameter. The lateral position of the drops is plotted versus time, and the axial velocity is plotted versus the axial location for Reynolds numbers of $Re_d = 25$ and

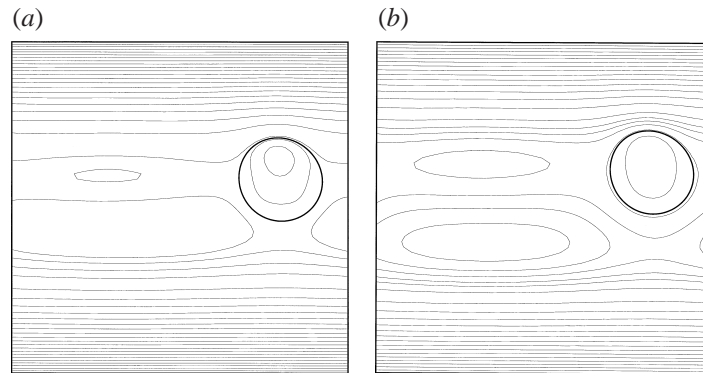


FIGURE 4. Streamlines for a drop at $Re_d = 0.25$, $Ca = 0.25$, $\alpha = 1$, and $\zeta = 0.125$. The viscosity ratio is $\gamma = 0.125$ for (a) and 1.0 for (b). The calculations were done using a 64×64 grid.

37. Even though the $Re_d = 25$ drop is released at a distance from the wall that is close to the equilibrium distance where it eventually will settle down, its path oscillates and the drop moves about 40 times the channel height before reaching steady state. As we found for the low-Reynolds-number case, the well-resolved drop lags behind the drop with the low resolution (0.7% of the axial velocity) and reaches an equilibrium position that is closer to the wall (0.6%). As the Reynolds number increases, the difference between the high-resolution and the 128^2 calculations increases and the transient oscillations observed in a 256^2 computation are damped. The accuracy of the computations was also examined for a lower viscosity ratio of $\lambda = 2$ and a Reynolds number equal to $Re_d = 37$ (see the bottom frames of figure 3). The periodic oscillations observed in this case reach a larger amplitude for the 256^2 grid, and the drop on the 128^2 grid is out of phase with the drop on the 256^2 grid. Because of the phase difference, a comparison of the flow at the same time results in large differences. If the comparison is done when the drops are at the same lateral positions, however, the flow patterns are similar. A calculation using a 256^2 grid takes about 9 CPU seconds for each time step on an UltraSPARC 170E SUN workstation for $Re_d = 37$. The total number of time steps required for the computation is about 439 000, resulting in a total of 3 951 000 CPU seconds.

4.2. Lateral migration of a liquid drop in the small inertia limit

We start by studying the motion of a deformable drop in two-dimensional Poiseuille flow by a series of simulations in the limit of small inertia. Since the flow is dominated by viscous effects, the proper non-dimensional number is the capillary number, expressing the ratio of viscous stress to surface tension. The theory of Chan & Leal (1979) is limited to small deformation and small drops, but the simulations allow arbitrary deformation and finite drop sizes. It is possible to select parameters where the limitations of the theory are approximately satisfied, but exact agreement cannot be expected since our simulations in this section are for two-dimensional drops.

To investigate the dependence of the migration on the viscosity ratio, we conduct simulations at $\lambda = 0.125$ and $\lambda = 1$. The relative size of the drop is $\zeta = 0.125$, and two different Reynolds numbers are considered, $Re_d = 0.25$ and 1.0.

We first consider the lower Reynolds number case. The calculations are done on a 64^2 grid. The capillary number is $Ca = 0.25$, so the deformation of the drop is small, and the density ratio is $\alpha = 1$. Figure 4 shows the drop contours and the streamline patterns for two drops with viscosity ratios $\lambda = 0.125$ and $\lambda = 1$ at time $t = 36.9$.

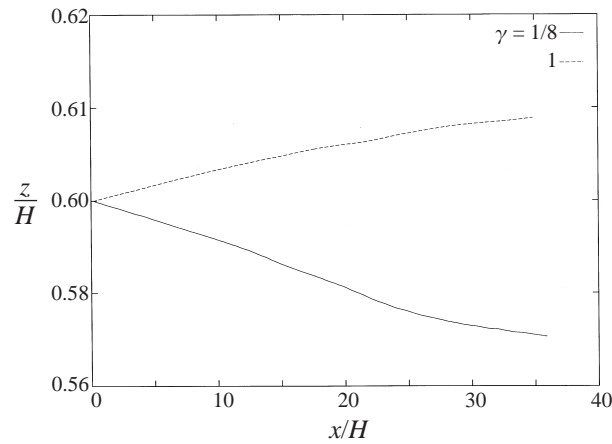


FIGURE 5. The lateral position of the drops in figure 4, measured from the lower wall, versus the axial location.

The centre of the recirculation pattern inside the high-viscosity drop is close to the centre of the drop, but the centre of recirculation of the low-viscosity drop is close to the wall. The lateral positions of the drops are plotted versus the axial location in figure 5. The low-viscosity drop migrates toward the centreline, and the high-viscosity drop migrates away from the centreline, in agreement with the predictions of Chan & Leal, even though the relative size of the drop is not small. The lateral migration is, however, very weak, and it would take a long time for the drop to move to an equilibrium position.

Since we use explicit time-stepping, simulations at a very low Reynolds number require very small time steps for stability. We have therefore increased the Reynolds number to $Re_d = 1$ to reach an equilibrium position using less computer time. The computations are done on a 128^2 grid. Figures 6 and 7 show results of four simulations: two with $Ca = 1$ and a viscosity ratio of (a) $\lambda = 1$, and (b) $\lambda = 0.125$; and two for $Ca = 2$ and $\lambda = 0.125$, but different density ratios ($\alpha = 0.125$ in (c), $\alpha = 1$ in (d)). Since Ca is higher here than for the drops in figure 4, the drops deform more. Figure 6 shows the lateral position measured from the lower wall and the axial velocity of the drop versus the axial location. The initial positions of drops (a), (b) and (d) are the same; drop (c) is released closer to the wall. The low-viscosity drop in (b) migrates toward the centre of the channel, but the high-viscosity drop (a) migrates toward the wall. These results are again in agreement with the theoretical predictions of Chan & Leal for the viscosity dependence of the migration in the limit of small deformation. The drop that migrates to the wall reaches an equilibrium position at $Z_{eq}/H = 0.37$. The equilibrium position is not predicted by the theory since the effect of the wall is not included. Although an equilibrium position halfway between the centreline and the walls is seen at higher Reynolds numbers due to the Segre–Silberberg effect (§4.3), the present result is almost certainly due to the interplay of deformation and viscosity, since the drop moves to the centreline when its viscosity is decreased. This effect was also seen in the Stokes flow simulations of Zhou & Pozrikidis (1994) for $\lambda = 10$. Figure 7 shows drop contours and streamlines for cases (a) and (d) at times 56.8 and 55.6, respectively, when the drops have moved downstream approximately 50 times the height of the channel. The shape of drop (d) (as well as drop (c), not shown) agrees qualitatively with the predicted shape of

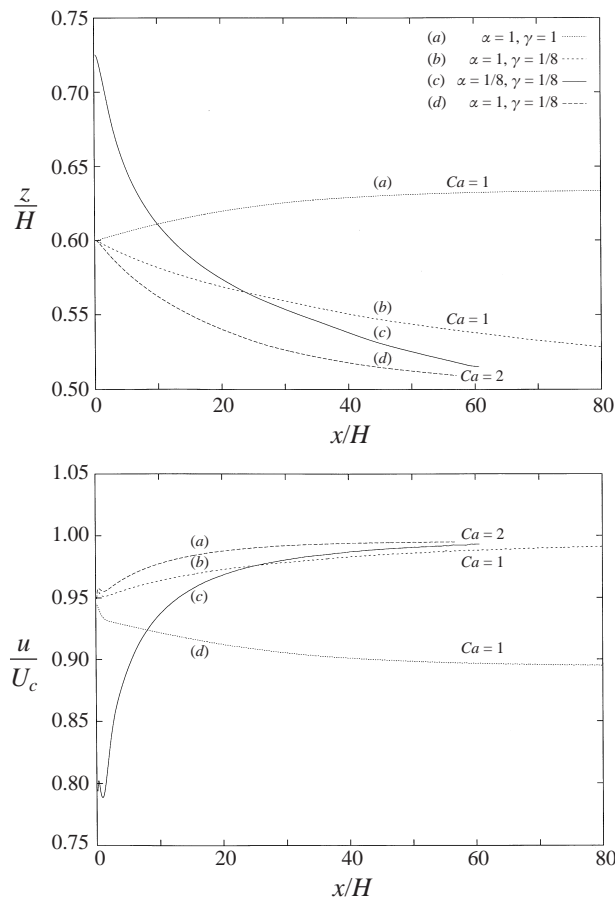


FIGURE 6. Lateral position and axial velocity versus the axial position for several drops with $Re_d = 1$ and different viscosity and density ratios.

Chan & Leal for a deformed drop moving at the channel centreline. However, the deformation is larger here since the relative size of the drop is larger.

The effect of deformation on the migration of the drop can be investigated by considering drops (b) and (d) in figure 6, which have different capillary numbers but the other parameters the same. The more deformable drop (d) migrates faster to the centre of the channel. Drops at a low-viscosity ratio, but with different density ratios ($\alpha = 0.125$ and $\alpha = 1$) both migrate to the centre of the channel (c and d) at about the same rate, confirming that the density ratio does not play a significant role in the drop migration when flow inertia is small.

The axial velocities of the drops are plotted versus the axial location in figure 6. As predicted by Chan & Leal, the drop always lags behind the undisturbed flow. Drops with a higher capillary number move slightly faster than drops with a lower capillary number, but the slip velocity is small in both cases.

Experimental investigations of the motion of a single drop in pressure-driven channel flow (see e.g. Karnis & Mason 1967; Goldsmith & Mason 1961, 1962) have shown that the drop moves away from the channel wall. For low viscosity ratios the drops reach the centre of the channel. This is in agreement with the theory of Chan & Leal and the simulations presented here. Hiller & Kowalewski (1987) conducted

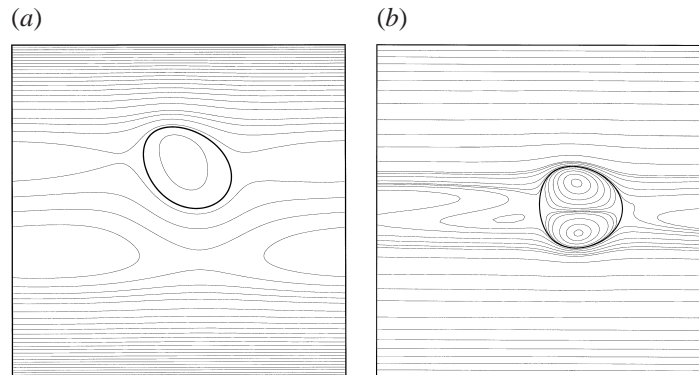


FIGURE 7. Streamlines for a drop at $Re_d = 1$, $\alpha = 1$, and $\zeta = 0.125$, (a) $\gamma = 1$, $We = 1$ and $Ca = 1$, (b) $\gamma = 0.125$, $We = 2$ and $Ca = 2$ (corresponding to drops (a) and (d) in figure 6). Notice that the streamlines are not equally spaced in frame (b).

experiments on a dilute suspension of drops with different viscosity ratios and found that for low-viscosity drops ($\lambda = 0.1$), the drop number density is eventually highest at the centreline, but for moderate viscosity ratios ($\lambda = 1$), the highest concentration was located between the wall and the centre. This is, again, in agreement with the results found here and with the theory of Chan & Leal. Although the present simulations are only two-dimensional and therefore not completely comparable with the predictions of Chan & Leal and with the experimental results, we will show in §4.4 that many aspects of the three-dimensional evolution of drops in a channel are well predicted by two-dimensional simulations.

To examine the effect of the drop size, we have done simulations with larger drops. Larger drops disturb the flow more, and we have therefore used a rectangular channel that is three times longer than its height for these simulations. Figure 8(a) shows the lateral position of four drops at small Reynolds numbers plotted against time. For drops (e), (f), (g), $\zeta = 0.375$ and for drop (h), $\zeta = 0.4375$. The density ratio is unity for all drops. To examine the significance of inertia, the Reynolds number was reduced by a factor of four from drop (e) where $Re_b = 4$ to $Re_b = 1$ for drop (f). The results are essentially identical, suggesting that inertia effect is negligible. The effect of the viscosity ratio can be seen by comparing the motion of drop (f) where $\lambda = 1$, to drop (g) where $\lambda = 0.125$. Unlike small drops, both large drops migrate to the centreline. The largest drop (h) migrates faster to the middle of the channel. The capillary number for this drop is smaller, but the capillary number based on the shear velocity ($U_c a/H$) is the same for all drops. Figure 8(b) shows the streamlines at steady state for drop (h). The streamlines show that the region behind the drop is composed of two circulation zones that are symmetric with respect to the axial direction. The drop is stretched in the axial direction and has a sharp leading edge and a flattened trailing edge. The shape of drop (h) is in qualitative agreement with those seen in the experiments performed by Olbricht & Kung (1992) in the limit of creeping flow. The flow rate through the channel, expressed by the ratio of the actual flow rate in the presence of the drop to the undisturbed flow rate (Q_d/Q_o) is the same for drops (e) and (f), $Q_d/Q_o = 0.95$. However, the flow rate increases for drop (g), $Q_d/Q_o = 1.02$. This is consistent with the theoretical predictions of Brenner and Bungay (see Olbricht 1996) who showed that the extra pressure drop for constant flow rate due to the presence of the drop is a function of the viscosity ratio and the drop size. The theory, in

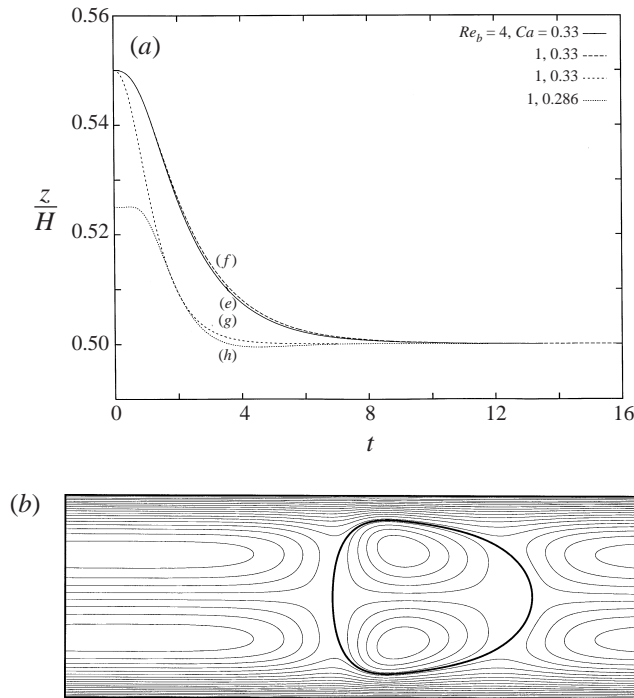


FIGURE 8. (a) The lateral position versus time for large drops at small Reynolds numbers, and (b) the streamlines at steady state for drop (h). The density ratio is $\alpha = 1$ for all cases. The viscosity ratio is also $\gamma = 1$ for all cases except for drop (g) where $\gamma = 0.125$. The non-dimensional size of the drop is $\zeta = 0.375$ for drops (e), (f), (g), and 0.4375 for drop (h).

particular, shows that the extra pressure drop can be negative for large drops and small viscosity ratios.

4.3. Lateral migration of a liquid drop at moderate Reynolds numbers

In this subsection, our study of the motion of a liquid drop is extended to higher Reynolds numbers, and the effects of the various governing parameters are examined in detail.

4.3.1. Effect of drop deformation

For drops in Stokes flow, deformation is the only means of lateral migration. To illustrate the role of deformation for non-zero Reynolds numbers, in figure 9(a) we show the equilibrium shapes and positions of three drops with $We = 0.5, 4,$ and 16 , all for $Re_d = 10, \alpha = \lambda = 8,$ and $\zeta = 0.125$. The particle Reynolds number and the channel Reynolds number are $Re_p = 0.625$ and $Re_b = 40.0$. As the Weber number is increased, the drops are more deformed. The streamlines at steady state are shown in figure 9(b) for the most deformed drop ($We = 16$). Those should be compared with figure 2, where streamlines are shown for $We = 0.5$. The flow patterns are similar, but while the major axis of the $We = 4$ drop is oriented at about 45° with respect to the channel wall, the major axis of the $We = 16$ drop is aligned more with the flow direction.

The lateral position of the drop is plotted versus the axial location in figure 10(a). The equilibrium distance from the upper wall is $Z_{eq}/H = 0.28$ for the nearly circular drop, which is somewhat higher than the value predicted by the perturbation theories of Ho & Leal (1974), Vasseur & Cox (1976), and Schonberg & Hinch (1989) (0.2,

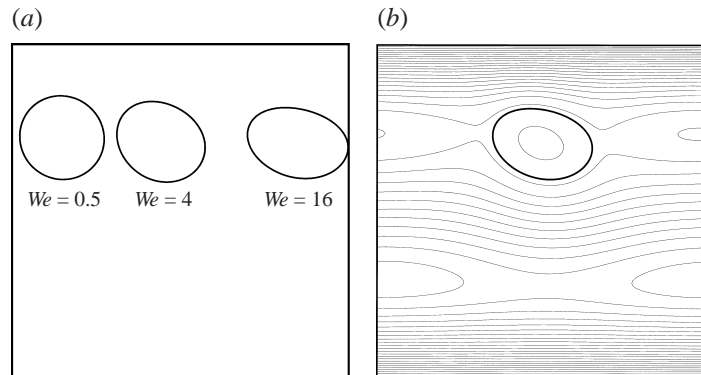


FIGURE 9. (a) Equilibrium position and shapes of drops at $Re_d = 10$, $\alpha = \gamma = 8$, at different Weber numbers. The initial position is the same for all drops. (b) Streamlines for the $We = 16$ drop.

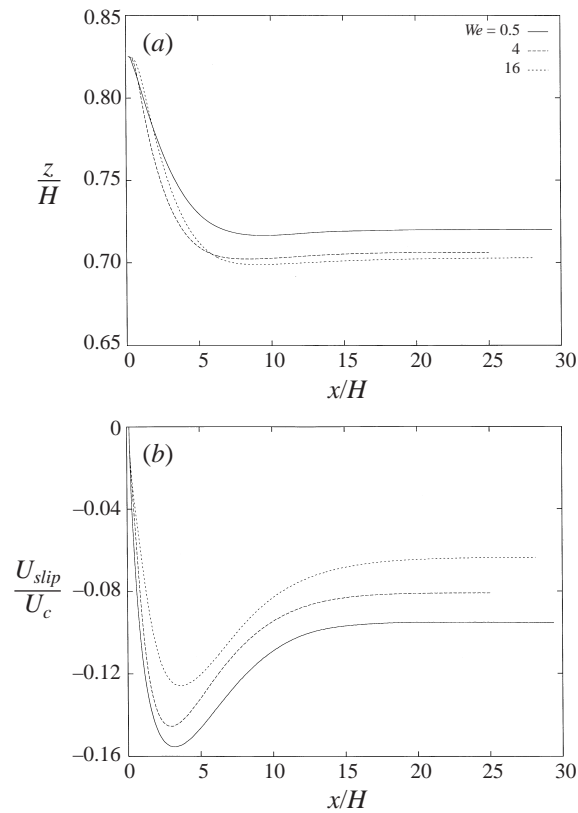


FIGURE 10. (a) The lateral position and (b) slip velocity, versus the axial position, for the drops shown in figure 9(a).

0.19 and 0.185, respectively) in the limit of a small particle and small Reynolds number. However, our result is close to that of the two-dimensional simulations of Feng *et al.* (1994b), who found $Z_{eq}/H = 0.252$ for neutrally buoyant solid particles. Ho & Leal (1974) and Feng *et al.* (1994b) both discussed the mechanism determining the equilibrium position. The flow through the gap between the particle and the

wall results in a repulsive lubrication force, called ‘geometric blocking’ by Feng *et al.* (1994*b*), that increases with the particle size. However, the particle always has a negative slip velocity and lags behind the undisturbed flow. The negative slip velocity and the curvature of the velocity profile generate a force that drives the particle away from the centre of the channel. Since the deformed drop is thinner, the difference in flow velocity across the drop is smaller than for a spherical drop. The force pushing it to the wall is therefore smaller and the equilibrium position is closer to the centreline. This effect, however, is small. The ‘slip’ velocities, defined as the axial velocity of the drop minus the undisturbed fluid velocity at the drop centroid, are plotted in figure 10(*b*). The drops always lag behind the undisturbed flow in agreement with the theoretical predictions of Chan & Leal (1979) for creeping flow and the numerical simulations of Feng *et al.* (1994*a, b*) for rigid particles at moderate Reynolds numbers. The slip velocity is smallest for the most deformable drop ($We = 16$) since it exhibits the least resistance to the flow. The reduced slip velocity, as well as the slight change in the equilibrium position, causes the deformed drop to move considerably faster down the channel than the undeformed drop.

Experiments focusing on the effect of deformability have all been done at much smaller Reynolds numbers than the ones considered here. In the studies of Goldsmith & Mason (1962) and Karnis & Mason (1967), where the Reynolds number was essentially zero ($Re_p = 10^{-6}$), the drops were found to move toward the centreline. At a higher Reynolds number (but still much smaller than unity, $Re_p = 0.0004$ to 0.007), Karnis *et al.* (1963) found that drops with viscosity ten times the suspending fluid viscosity move to the centreline whereas more viscous drops ($\lambda = 50$) move to a position halfway between the centre and the wall, in agreement with results found for solid particles. Karnis *et al.* argued that the increased viscosity leads to smaller deformation and that the different behaviour was the result of the increased deformability. Since drops can migrate in zero Reynolds number flows only if they deform, it is likely that the final position of a deformable drop at non-zero Reynolds numbers is the result of competition between deformability and inertia. At the Reynolds numbers examined here, inertial effects are dominant and the equilibrium position is determined by the Segre–Silberberg effect.

4.3.2. Effect of the Reynolds number

To examine the effect of the Reynolds number, in figure 11 we plot the lateral position of the drop versus the axial location for Reynolds numbers $Re_d = 5, 10, 25, 37$, and 50, for $We = 0.5$, $\alpha = \lambda = 8$, and $\zeta = 0.125$. At low Reynolds numbers the drops approach the equilibrium position monotonically. As the Reynolds number is increased, the drops overshoot the equilibrium position and oscillate several times before settling down. The equilibrium position also moves slightly closer to the wall. The amplitude of the oscillations increases with the Reynolds number and the rate of decay decreases. At $Re_d = 25$, the oscillations have not died out after the drop has moved more than 90 channel heights downstream. The low Reynolds number results are in agreement with the perturbation theory of Schonberg & Hinch (1989), who found that the equilibrium position of rigid spheres moves closer to the walls as the Reynolds number increases: As the Reynolds number is increased, viscous effects are reduced, the lubrication forces between the wall and the drop are also reduced, so the drop moves closer to the wall.

Indirect experimental evidence suggests that drops oscillate at high Reynolds numbers. Segre & Silberberg (1962*b*) conducted experiments using a multi-particle system with nearly neutrally buoyant solid spheres and relatively low volume fractions. They

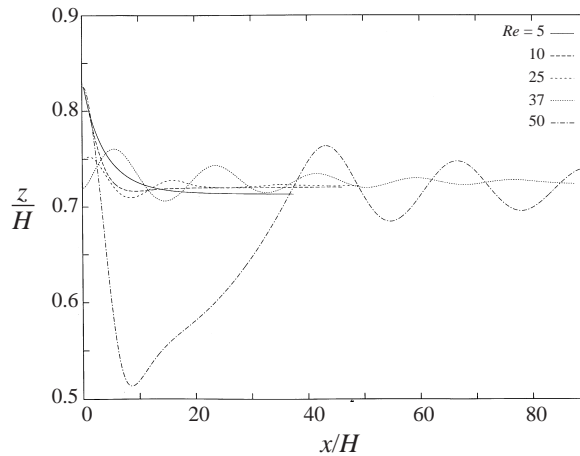


FIGURE 11. The lateral position versus the axial location of a drop with $\alpha = \gamma = 8$, $We = 0.5$, $\zeta = 0.125$ and five different Reynolds numbers. The Reynolds number is based on the centreline velocity and the drop diameter.

observed that concentrated layers of particles, found around the equilibrium position at low Reynolds numbers, became blurry and their thickness increased as the Reynolds number increased. This could be due to unsteady motion of the particles. The width of the particle-free layer adjacent to the wall also decreased and the rate at which the concentration of particles decayed from the centreline to the equilibrium position was reduced. At very high channel Reynolds numbers ($Re_b = 346-1388$), the layer is completely smeared out.

4.3.3. *Effect of the viscosity ratio*

In experiments, where the behaviour of drops of different fluids is examined, the ratio of the drop viscosity to the viscosity of the suspending fluid is the most important quantity that is changed (assuming that the size of the drops and the pressure gradient remains constant). In this section, we examine the effect of the viscosity ratio for a small deformation ($We = 0.5$) and moderate Reynolds numbers. The effect of the viscosity ratio for very small Reynolds numbers was examined in §4.2.

In figure 12, the lateral velocity of a single drop is plotted versus its lateral position for two viscosity ratios ($\lambda = 2$ and 8) and four different Reynolds numbers ($Re_d = 10, 25, 37$, and 50). For $Re_d = 10$, (a), the drops move nearly monotonically to the equilibrium position, and the low-viscosity drop ends up closer to the wall. As the Reynolds number is increased to $Re_d = 25$, (b), both drops significantly overshoot the equilibrium position, and the low-viscosity drop continues to oscillate even after it has moved downstream over 60 channel heights. The motion of the viscous drop, on the other hand, is damped more quickly. Although the low-viscosity drop has not completely settled down, it is clear that its equilibrium position will be slightly closer to the wall than that of the more viscous drop, as in the case of $Re_d = 10$. In (c) the Reynolds number has been increased to 37 and the amplitude of the oscillation is larger than in (a) and (b). While the oscillations of the $\lambda = 8$ drop are eventually damped, the oscillations of the low-viscosity drop ($\lambda = 2$) are not. For $Re_d = 50$ (d), the oscillations of the more-viscous drop are damped and it moves slowly to an equilibrium position. The less-viscous drop not only fails to reach a steady state, but

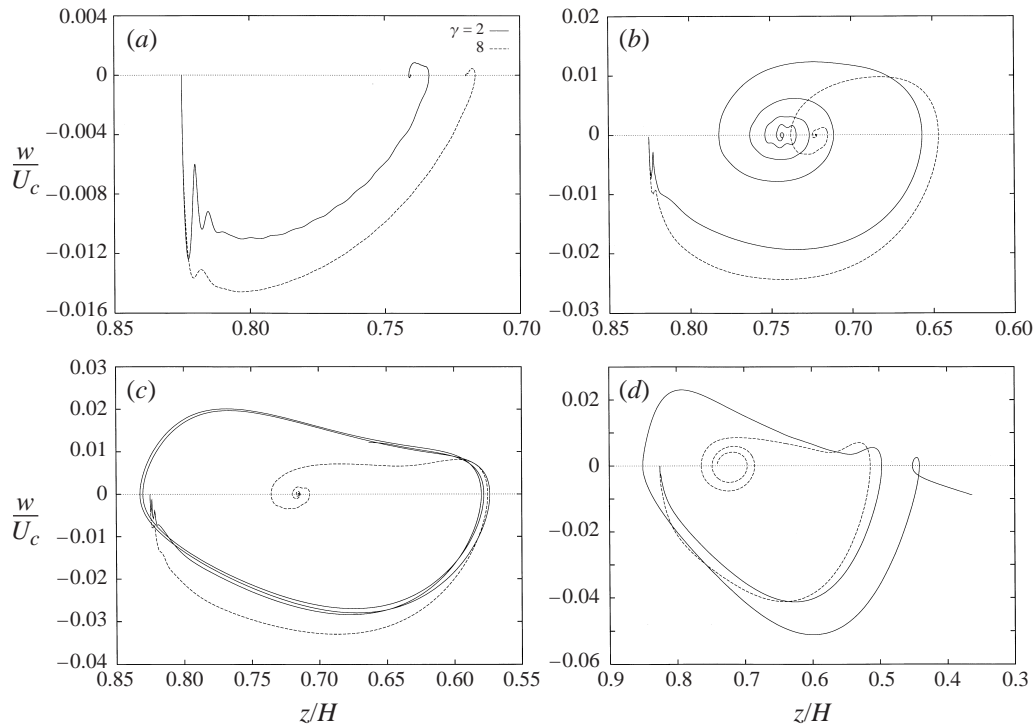


FIGURE 12. The w -velocity versus the z -coordinate of a drop at four different Reynolds numbers: $Re_d = 10$ (a), 25 (b), 37 (c), and 50 (d). Other flow parameters are: $\alpha = 8$, $We = 0.5$, and $\zeta = 0.125$.

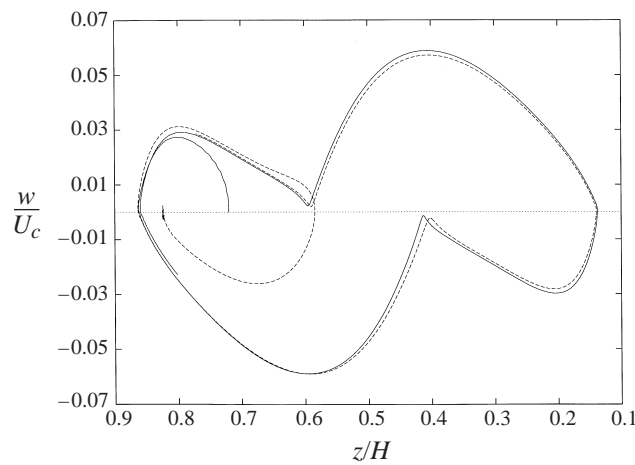


FIGURE 13. The w -velocity versus the z -coordinate of two drops with different initial positions with $Re_d = 37$, $\alpha = 8$, $\gamma = 1$, $We = 0.5$, and $\zeta = 0.125$. Calculations were done on a 256×256 grid.

actually has moved over to the other side of the channel by the time the simulation was terminated.

To examine the behaviour at even lower viscosity, we repeated the simulation for $Re_d = 37$ with $\lambda = 1$. Figure 13 shows the lateral velocity versus the lateral position for two drops with different initial positions. The drop initially located closer to the centreline immediately moves to the closest wall, bounces back across the centreline,

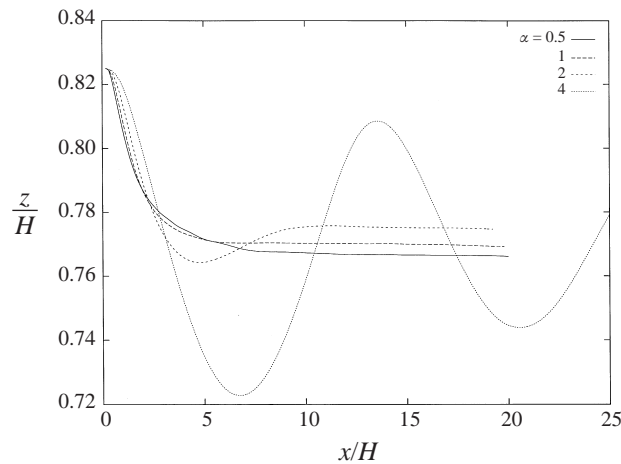


FIGURE 14. Effect of the density ratio on the equilibrium position of a drop at $Re_d = 37$, $We = 0.5$, and $\gamma = 1$. Calculations are done on a 256×256 grid.

slows down to nearly zero velocity at about halfway between the wall and the centreline, and is then thrown to the other side to repeat the motion. The other drop, initially located close to the wall, first moves to a position about halfway between the wall and the centreline, but is then pushed to the wall and follows the same path as the first drop.

The reason why the equilibrium position of the low-viscosity drops is closer to the wall can be explained as follows: A high drop viscosity slows down the ambient flow on the side of the drop facing the wall, thereby increasing the viscous blocking (lubrication force) of the flow between the wall and the drop, and causing the equilibrium position to move further away from the wall. The same effect is seen for solid particles where a freely rotating sphere is found to be closer to the wall than a sphere that is prevented from rotating (Feuillebois 1989). The oscillatory motion seen for low-viscosity drops at high Reynolds numbers is likely to be due to the reduced dissipation.

Our results differ from those of Karnis *et al.* (1966*a, b*) who found that drops with very low-viscosity ratios move to the axis of the channel. However, their Reynolds number was very low (typically much smaller than unity) and we have found (§4.3.1) that increased deformability does not change the equilibrium position of the drop significantly in the Reynolds number range considered in this section. We therefore believe that the main reason for the different behaviours is the difference in the Reynolds number. At low Reynolds numbers (less than unity), deformation can drive the drops to the centreline, but at higher Reynolds numbers ($Re_d = 10$), inertia moves the drop to an equilibrium position at about halfway between the centreline and the wall.

The computations presented in this section were carried out using 128^2 and 256^2 grids and some of the runs have been repeated with drops starting from different initial conditions. The results shown in figure 12 remain essentially unchanged.

4.3.4. Effect of the density ratio

The effect of the density ratio on the lateral migration of a drop was examined by carrying out four simulations with $\alpha = 0.5, 1.0, 2.0$, and 4.0 , all for $Re_d = 37$, $We = 0.5$ and $\lambda = 1$. Figure 14 shows the lateral position versus the axial location of the centre

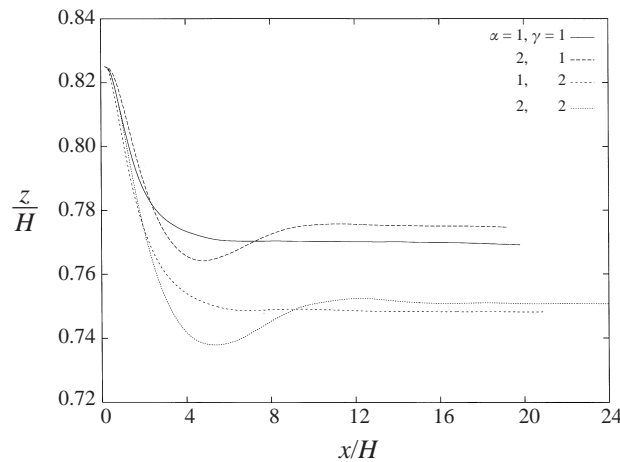


FIGURE 15. Comparison between the effect of the viscosity and the density ratio on the equilibrium position of a drop. The flow conditions are: $Re_d = 37$ and $We = 0.5$.

of the drop. The transient motion of the drop is strongly affected by the density ratio. The low-density drops approach an equilibrium position monotonically, whereas the heavier drops overshoot; the heaviest drop ($\alpha = 4$) undergoes several slowly decaying oscillations. To confirm that the oscillations are indeed damped, this simulation was carried out for a much longer time. For the smaller density ratios, it is clear that the equilibrium position of the heavier drops is slightly closer to the wall. We note that increasing the density of the drop has the same effect as decreasing the viscosity of the drop, and this suggests that it is the high Reynolds number of the drop that promotes oscillatory motion. However, changes in the viscosity ratio have stronger effects, as shown in figure 15, where the lateral position of the drop versus distance travelled down the channel is plotted for two density ratios and two viscosity ratios.

4.3.5. Effect of the drop size

The effect of the size of the drop is shown in figure 16, where the lateral position of the drop is plotted versus the axial position for seven drops with different sizes. The flow parameters are: $Re_b = 40$, $We = 0.5$, $\alpha = \gamma = 1$, and $\zeta = 0.09, 0.1875, 0.281, 0.375$, and 0.4375 for drops 1, 2, 3, 4 and 5, respectively. The Weber number is higher for drop 6, $We = 4$, and the Reynolds number is smaller for drop 7, $Re_b = 13.3$. Other parameters for drops 6 and 7 are the same as for drop 4. To reduce the effect of the periodic boundary condition, the length of the computational domain was increased to three times the channel height in these simulations. For large drops, the periodic length can have a significant effect, but as will be shown in §4.3.6, the effect is small for small drops. The domain was resolved by a 384×128 grid. The steady-state shapes and positions of drops 1, 2, 3, 4 and 5 are also shown in figure 16. Since the Weber number is low, the drops remain nearly circular. As the drops get larger, the velocity difference across the drop increases and therefore also the force pushing the drops to the wall. The gap between the drop and the wall therefore decreases. However, since the radius of the drop is increasing, the centroid of the drop moves away from the wall. When the drop diameter is comparable to the channel height (drop 5), the equilibrium position moves to the channel centreline. Reducing the Reynolds number for drop 4 (drop 7) moves the equilibrium position closer to the centreline, but not all the way. Making drop 4 more deformable (drop 6) results in an equilibrium

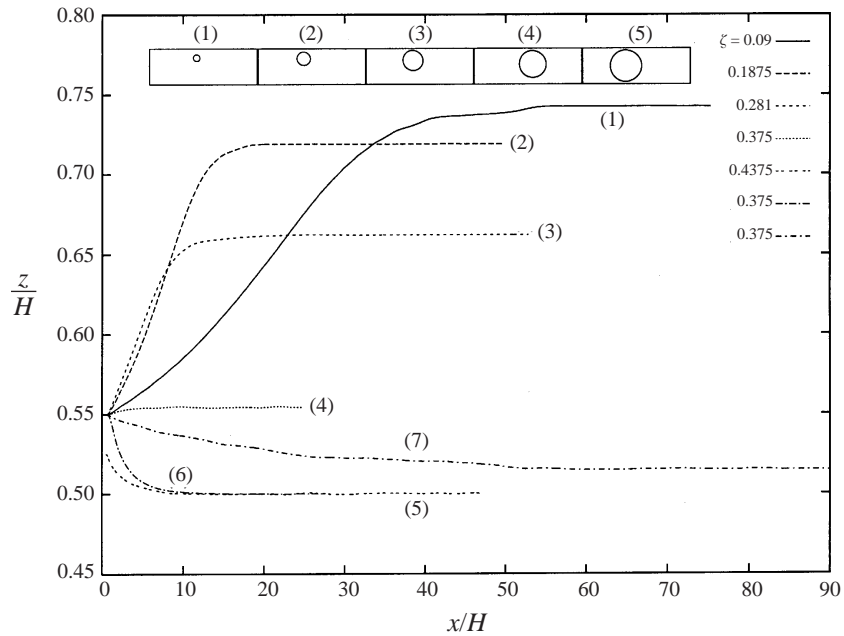


FIGURE 16. Effect of the drop size on the lateral migration of a drop in a plane Poiseuille flow. The flow conditions for drops 1, 2, 3, 4, and 5 are: $Re_b = 40$, $\alpha = \gamma = 1$, and $We = 0.5$. Drop 6 has a higher Weber number ($We = 4$), and the Reynolds number is lower for drop 7 ($Re_b = 13.3$). Computations are done in a rectangular channel with a length that is three times its height. The resolution is 384×128 points.

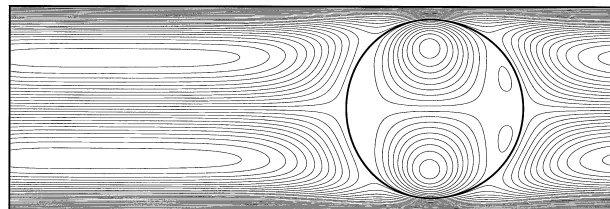


FIGURE 17. Streamlines at steady state for drop 5 in figure 16.

position exactly on the centreline. This strong dependence of the equilibrium position on the Weber and Reynolds number was not seen for smaller drops at high enough Reynolds numbers. However, for very low Reynolds numbers large deformable drops move to the centreline. Large drops with a diameter comparable to the channel height therefore always migrate to the channel centreline at small and moderate Reynolds numbers. The streamlines for drop 5 are plotted in figure 17. The streamlines show a nearly symmetric pattern with respect to the centreline at steady state.

The results are in agreement with the experiments of Karnis *et al.* (1966*b*) who examined the equilibrium position of particles of different sizes in a pipe at relatively low Reynolds numbers and found the equilibrium positions $Z_{eq}/H = 0.23, 0.33, 0.36$, and 0.43 for rigid spheres with $\zeta = 0.0775, 0.2, 0.2625$, and 0.389 , respectively. For liquid drops with viscosity ratio of $\lambda = 50$, where the drops behaved like solid spheres, the equilibrium position was $Z_{eq}/H = 0.235$ and 0.25 for drops of size $\zeta = 0.04625$ and 0.06 , respectively. Comparison between our results and the experimental data is shown in figure 18. Our results are for nearly circular drops, but the viscosity

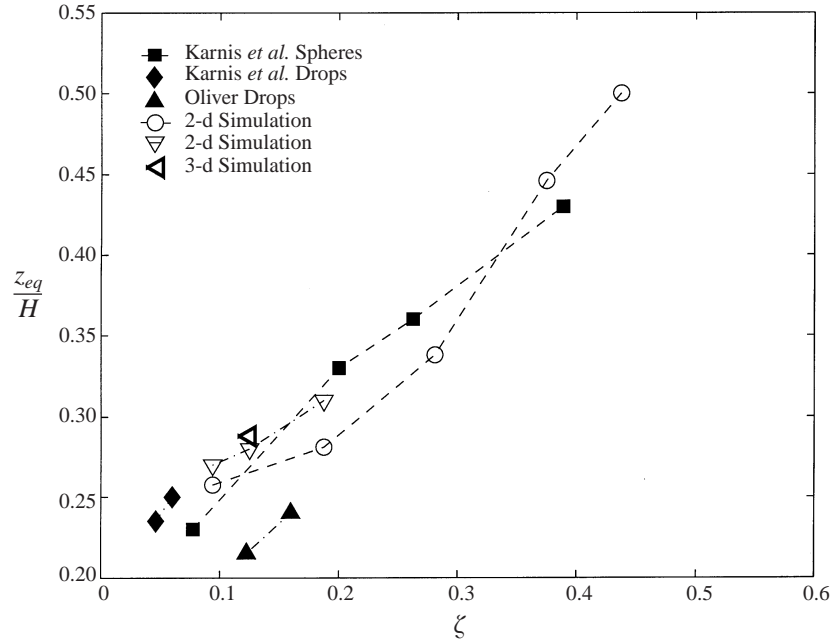


FIGURE 18. Comparison between experimental data and simulations for the equilibrium position of a drop as a function of the drop size: the solid symbols represent the experimental data; the open circles are for two-dimensional simulations at $Re_b = 40$, $\alpha = \gamma = 1$, and $We = 0.5$ in a long channel; the open triangles are for two-dimensional simulations at $Re_d = 10$, $\alpha = \gamma = 8$, and $We = 0.5$ in a square channel; the three-dimensional simulation is at $Re_d = 10$, $\alpha = \gamma = 8$, and $We = 0.5$.

ratios ($\lambda = 1$ and 8) are lower than in the experiments. This figure also shows the experimental data of Oliver (1962) for rigid spheres at a relatively high Reynolds number ($Re_b = 100$ to 500). Although the agreement is reasonably good, we note that most of the numerical results are for two-dimensional drops whereas the experimental results are for fully three-dimensional drops. The equilibrium position of one three-dimensional drop, which is nearly identical to that of a two-dimensional drop, is also shown in figure 18.

As the equilibrium position moves closer to the centre, the axial velocity of the drops increases. Large particles are therefore advected faster than small particles for a given pressure drop. We note that the equilibrium positions predicted by perturbation theories, for drops that are much smaller than the channel width, are always closer to the channel walls than what is predicted by the present simulations.

4.3.6. Effect of periodicity

To investigate the effect of the periodic boundary condition on the migration of a drop, we repeated a few simulations using channels of different lengths (L). In figure 19, we present the lateral position versus the axial location of drops with two different sizes: $\zeta = 0.125$, and 0.375 . The channels have three different sizes: $L/H = 1, 2$ and 3 . Comparison between the equilibrium positions of the drop with $\zeta = 0.125$ shows that when the channel length is doubled from $L/H = 1$ to $L/H = 2$, the equilibrium position changes by 1%. Increasing the channel length further has essentially no effect. For the large drop, $\zeta = 0.375$, the equilibrium position changes by 6% as the

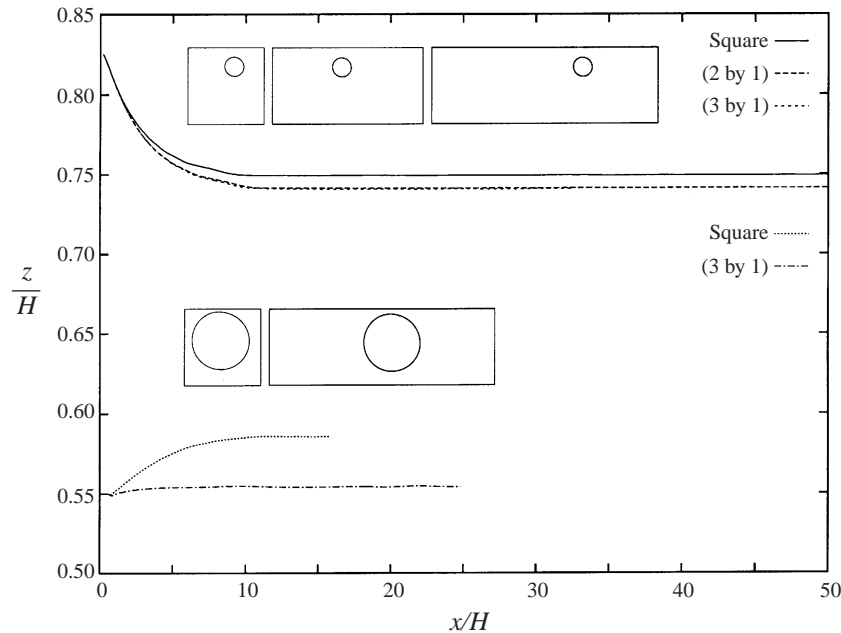


FIGURE 19. Effect of the channel length on the lateral migration of a drop in a plane Poiseuille flow. Results are for two different drop sizes: $\zeta = 0.125$, and 0.375 . The channels are: a square, a rectangle whose length is twice its height, and a rectangle with a length that is three times its height. The flow conditions are: $Re_b = 40$, $\alpha = \gamma = 1$, $We = 0.5$.

channel is extended from $L/H = 1$ to $L/H = 3$. As a result, the effect of the periodic boundary condition on the equilibrium position of a drop is small if the drop size is small. The insensitivity of the results to the length of the period is in agreement with Stokes flow predictions, which show that the disturbance due to a stokeslet between parallel plates decays rapidly upstream and downstream (see, for example, Liron & Shahar 1978, and references therein).

4.4. Simulations of three-dimensional flow

The results for two-dimensional flows presented in the previous sections were obtained using relatively fine grids, and the simulations were carried out for a relatively long physical time to obtain steady-state solutions. Three-dimensional simulations of the same complexity require much longer computational time, and we have only conducted a few three-dimensional simulations at a low Reynolds number using relatively coarse grids. To make the conditions of the three-dimensional and the two-dimensional simulations as similar as possible, and to reduce the computational time, we use a domain that is relatively narrow in the y -direction ($0.375H$). The grid resolution is $64 \times 24 \times 64$ in the x -, y - and z -directions, respectively. In figure 20, the drop and steady-state streamlines in a plane through the centre of the drop ($y = 0.1875H$) are shown for $Re_d = 10$, $We = 0.5$, $\alpha = \lambda = 8$, and $\zeta = 0.125$.

In figure 21, a comparison between the three-dimensional drop shown in figure 20 and a two-dimensional simulation with the same parameters is shown by plotting the lateral position and the axial velocity of the drop versus the axial position. The two-dimensional simulation was done using two resolutions to show the effect of discretization. The grid resolution for the three-dimensional case and for the low-

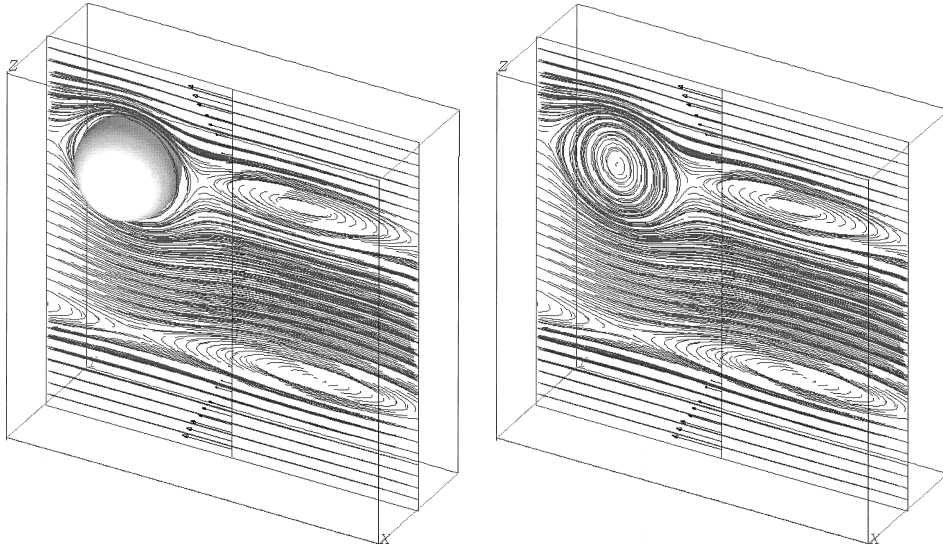


FIGURE 20. The drop and steady-state streamlines for three-dimensional simulation at $Re_d = 10$, $\alpha = \gamma = 8$, and $We = 0.5$.

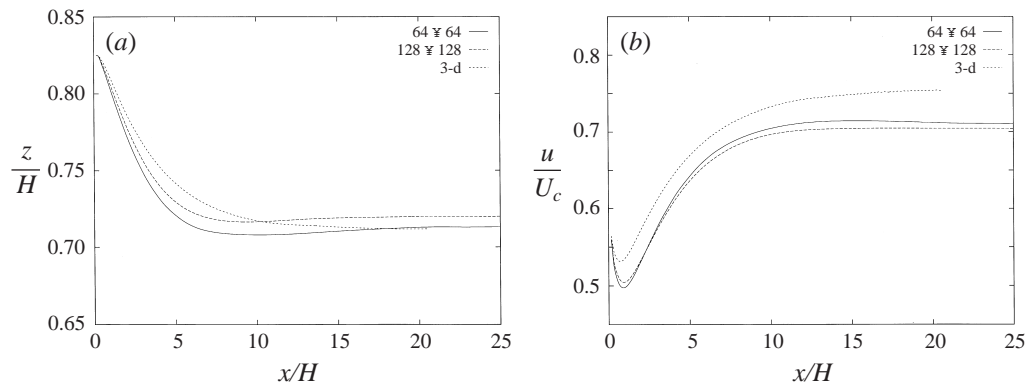


FIGURE 21. Comparison between two- and three-dimensional simulation of a drop at $Re_d = 10$, $We = 0.5$, and $\alpha = \gamma = 8$: (a) the lateral position of the drop and (b) the axial velocity versus the axial position.

resolution two-dimensional calculation are the same. The equilibrium position of the three-dimensional drop agrees well with the two-dimensional one at the lower resolution, but the three-dimensional drop has a higher translational velocity. This is likely to be due to the smaller disturbance of the flow field caused by the three-dimensional drop, which leads to a lower drag compared to the two-dimensional one.

The effect of the viscosity ratio is shown in figure 22, where the lateral position of a three-dimensional drop is plotted versus its axial location, for viscosity ratios of $\lambda = 2$ and 8. As the viscosity ratio is reduced the three-dimensional drop migrates to an equilibrium position closer to the wall, in agreement with the result for the two-dimensional drops. This effect has already been discussed for two-dimensional simulations in § 4.3.3.

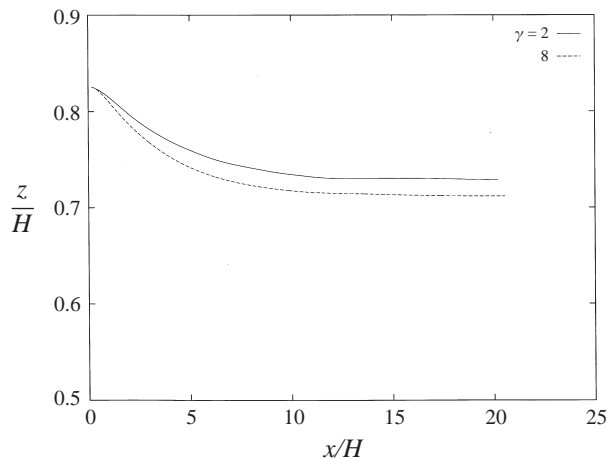


FIGURE 22. The effect of the viscosity ratio on the equilibrium position of a three-dimensional drop with $Re_d = 10$, $\alpha = 8$, and $We = 0.5$. The lateral position is plotted versus the axial position.

5. Conclusion

The motion of a single drop suspended in pressure-driven channel flow has been examined by numerical simulations which account for the effects of inertia, viscosity, and surface tension. Most of the simulations are confined to two-dimensional flow but a few three-dimensional flows are also considered.

Two sets of computations have been presented. For the first set (§4.2), the Reynolds number (Re_d) was $O(1)$ or lower. The results showed that the motion of a drop depends strongly on the ratio of the drop viscosity to the viscosity of the suspending fluid. A drop with a small viscosity moves toward the centreline at a rate that increases with the deformability of the drop, whereas a drop with viscosity comparable to the suspending fluid moves away from the centreline. Those results are in agreement with the theoretical predictions of Chan & Leal (1979) and computations of Zhou & Pozrikidis (1994), who found that the direction of migration of a drop in a Poiseuille flow depends on the viscosity ratio. Drops with $O(1)$ Reynolds numbers either move to the channel centreline, or reach a steady-state position between the centreline and the walls. The motion of the very low Reynolds number drop was not simulated for a long enough time for it to reach a well-defined equilibrium position.

For the second set of simulations (§4.3), the channel Reynolds number was much higher, $Re_d = 5-50$. In this range, small drops either settle to an equilibrium position about halfway between the centreline of the channel and the wall, or they undergo oscillatory motion. The exact position of the drops that settle down depends relatively weakly on the various physical parameters. Increasing the channel Reynolds number moves the equilibrium position slightly closer to the wall, whereas increasing the drop viscosity or making the drops more deformable (by lowering the Weber number) has the opposite effect. Increasing the drop density causes the equilibrium position to move closer to the wall, but only by a small amount. Increasing the size of the drop moves the equilibrium position closer to the centreline, although the gap between the wall and the drop surface is reduced. For the cases studied here, the changes in the equilibrium position are typically within a few percent. As the Reynolds number or the drop density is increased, or the viscosity of the drop is decreased, the drop first undergoes transient oscillations before reaching steady state. Once the Reynolds

number and/or the density are high enough and/or the viscosity ratio is low enough, the oscillations are not damped and the drops do not settle down. The oscillations consists either of motion around the equilibrium position confined to one half of the channel, or large-amplitude oscillations where the drop moves across the channel centreline. In the latter case, the drop pauses slightly as it passes the mid-point between the centreline and the wall, suggesting that this point is still an unstable equilibrium point. Large drops, whose diameters are comparable to the channel height, always move to the channel centreline, independent of the Reynolds number. Our results are in good agreement with experimental observations, particularly for drops that reach a steady-state lateral position (the Segre–Silberberg effect). For higher Reynolds numbers, however, the experimental data are not completely conclusive. Our two-dimensional computations are also in good agreement with the numerical results of Feng *et al.* (1994*b*), on the motion of a two-dimensional solid cylinder in a Poiseuille flow.

The results for the two-dimensional drops have been supplemented by two simulations of three-dimensional drops, but only for a modest Reynolds number, $Re_d = 10$, and a small computational domain. The results showed that the equilibrium position of the drops is close to the two-dimensional predictions, and that increasing the drop viscosity moved it slightly closer to the centreline, in agreement with two-dimensional predictions. We have, however, not confirmed the onset of oscillations at higher Reynolds numbers by simulations of three-dimensional drops.

This work was supported by the National Science Foundation under grant CTS-9503208 and by the National Aeronautics and Space Administration under contract NAG3-2162. The computations were done on the computers at the Center for Parallel Computing (CPC) at the University of Michigan. We would like to thank Dr Hal Marshall for his help with using the CPC facilities.

REFERENCES

- ADAMS, J. 1989 MUDPACK: Multigrid Fortran software for the efficient solution of linear elliptic partial differential equations. *Appl. Math. Comput.* **34**, 113–146.
- BENTLEY, B. J. & LEAL, L. G. 1986 An experimental investigation of drop deformation and breakup in steady, two-dimensional linear flows. *J. Fluid Mech.* **167**, 241–283.
- BERKMAN, S. & EGLOFF, G. 1941 *Emulsions and Foams*. Reinhold.
- BOZZI, L. A., FENG, J. Q., SCOTT, T. C. & PEARLSTEIN, A. J. 1997 Steady axisymmetric motion of deformable drops falling or rising through a homoviscous fluid in a tube at intermediate Reynolds numbers. *J. Fluid Mech.* **336**, 1–32.
- BRENNER, H. 1966 Hydrodynamic resistance of particles at small Reynolds numbers. *Adv. Chem. Engng* **6**, 287–438.
- CHAN, P. C. & LEAL, L. G. 1979 The motion of a deformable drop in a second-order fluid. *J. Fluid Mech.* **92**, 131–170.
- COX, R. G. & BRENNER, H. 1968 The lateral migration of solid particles in Poiseuille flow-I Theory. *Chem. Engng Sci.* **23**, 147–173.
- COX, R. G. & HSU, S. K. 1977 The lateral migration of solid particles in a laminar flow near a plane. *Intl J. Multiphase Flow* **3**, 201–222.
- COX, R. G. & MASON, S. G. 1971 Suspended particles in fluid flow through tubes. *Ann. Rev. Fluid Mech.* **3**, 291–316.
- COUILLETTE, C. & POZRIKIDIS, C. 1998 Motion of an array of drops through a cylindrical tube. *J. Fluid Mech.* **358**, 1–28.
- FENG, D. J., HU, H. H. & JOSEPH, D. D. 1994*a* Direct simulation of initial value problems for the motion of solid bodies in a Newtonian fluid. Part 1. Sedimentation. *J. Fluid Mech.* **261**, 95–134.
- FENG, D. J., HU, H. H. & JOSEPH, D. D. 1994*b* Direct simulation of initial value problems for the

- motion of solid bodies in a Newtonian fluid. Part 2. Couette and Poiseuille flows. *J. Fluid Mech.* **277**, 271–301.
- FENG, J. & JOSEPH, D. D. 1995 The unsteady motion of solid bodies in creeping flows. *J. Fluid Mech.* **303**, 83–102.
- FEUILLEBOIS, F. 1989 Theoretical results for the motion of solid spherical particles in viscous fluid. In *Multiphase Science and Technology* (ed. G. F. Hewitt, J. M. Delhay & J. M. Zuber), vol. 4, pp. 583–789. Hemisphere.
- GOLDSMITH, H. L. & MASON, S. G. 1961 Axial migration of particles in poiseuille flow. *Nature* **190**, 1095–1096.
- GOLDSMITH, H. L. & MASON, S. G. 1962 The flow of suspensions through tubes. I. Single spheres, rods and discs. *J. Colloid Sci.* **17**, 448–476.
- HILLER, W. & KOWALEWSKI, T. A. 1987 An experimental study of the lateral migration of a droplet in a creeping flow. *Exps. Fluids* **5**, 43–48.
- HO, B. P. & LEAL, L. G. 1974 Inertial migration of rigid spheres in two-dimensional unidirectional flows. *J. Fluid Mech.* **65**, 365–400.
- JEFFREY, R. G. & PEARSON, J. R. A. 1965 Particle motion in laminar vertical tube flow. *J. Fluid Mech.* **22**, 721–735.
- JOSEPH, D. D. & RENARDY, Y. Y. 1992 *Fundamentals of Two-Fluid Dynamics Part II: Lubricated Transport, Drops and Miscible Liquids*. Springer.
- KARNIS, A., GOLDSMITH, H. L. & MASON, S. G. 1963 Axial migration of particles in Poiseuille flow. *Nature* **200**, 159–160.
- KARNIS, A., GOLDSMITH, H. L. & MASON, S. G. 1966a The kinetics of flowing dispersions. I. Concentrated suspensions of rigid particles. *J. Colloid Sci.* **22**, 531–553.
- KARNIS, A., GOLDSMITH, H. L. & MASON, S. G. 1966b The flow of suspensions through tubes V. Inertial effects. *Can. J. Chem. Engng* **44**, 181–193.
- KARNIS, A. & MASON, S. G. 1967 Particle motions in sheared suspension. Part 23. Wall migration of fluid drops. *J. Colloid Interface Sci.* **24**, 164–169.
- KENNEDY, M. R., POZRIKIDIS, C. & SKALAK, R. Motion and deformation of liquid drops, and the rheology of dilute emulsions in simple shear flow. *Computers Fluids* **23**, 251–278.
- KHAYAT, R. E., LUCIANI, A. & UTRACKI, L. A. 1997 Boundary-element analysis of planar drop deformation in confined flow. Part 1. Newtonian fluids. *Engng Analysis with Boundary Elements* **19**, 279–289.
- LIRON, N. & SHAHAR, R. 1978 Stokes flow due to a stokeslet in a pipe. *J. Fluid Mech.* **86**, 727–744.
- MARTINEZ, M. J. & UDELL, K. S. 1990 Axisymmetric creeping motion of drops through circular channels. *J. Fluid Mech.* **210**, 565–591.
- OLBRICHT, W. L. 1996 Pore-scale prototypes of multiphase flow in porous media. *Ann. Rev. Fluid Mech.* **28**, 187–213.
- OLBRICHT, W. L. & KUNG, D. M. 1992 The deformation and breakup of liquid drops in low Reynolds number flow through a capillary. *Phys. Fluids A* **4**, 1347–1354.
- OLIVER, D. R. 1962 Influence of particle rotation on radial migration in the Poiseuille flow of suspensions. *Nature* **194**, 1269–1271.
- SAFFMAN, P. G. 1965 The lift on a small sphere in a slow shear flow. *J. Fluid Mech.* **22**, 385–400.
- SCHONBERG, J. A. & HINCH, E. J. 1989 Inertial migration of a sphere in Poiseuille flow. *J. Fluid Mech.* **203**, 517–524.
- SCHRAMM, L. L. 1992 *Emulsions Fundamentals and Applications in the Petroleum Industry*. American Chemical Society.
- SEGRE, G. & SILBERBERG, A. 1962a Behaviour of macroscopic rigid spheres in Poiseuille flow. Part 1. Determination of local concentration by statistical analysis of particles passages through crossed light beams. *J. Fluid Mech.* **14**, 115–135.
- SEGRE, G. & SILBERBERG, A. 1962b Behaviour of macroscopic rigid spheres in Poiseuille flow. Part 2. Experimental results and interpretation. *J. Fluid Mech.* **14**, 136–157.
- STONE, H. A. & LEAL, L. G. 1989 Relaxation and breakup of an initially extended drop in an otherwise quiescent fluid. *J. Fluid Mech.* **198**, 399–427.
- TACHIBANA, M. 1973 On the behavior of a sphere in the laminar tube flows. *Rheol. Acta* **12**, 58–69.
- TRYGGVASON, G., BUNNER, B., EBRAT, O. & TAUBER, W. 1998a Computations of multiphase flows by a finite difference/front tracking method. I Multi-fluid flows. In *29th Computational Fluid Dynamics*. Lecture Series 1998-03. Von Karman Institute for Fluid Dynamics.

- TRYGGVASON, G., ESMAEELI, A., MORTAZAVI, S., HAN, J. & HOMMA, S. 1998*b* Computations of multi-phase flows by a finite difference/front tracking method. II Applications. In *29th Computational Fluid Dynamics*. Lecture Series 1998-03. Von Karman Institute for Fluid Dynamics.
- UNVERDI, S. O. & TRYGGVASON, G. 1992*a* A front tracking method for viscous incompressible flows. *J. Comput. Phys.* **100**, 25–37.
- UNVERDI, S. O. & TRYGGVASON, G. 1992*b* Multifluid flows. *Physica D* **60**, 70–83.
- VASSEUR, P. & COX, R. G. 1976 The lateral migration of a spherical particle in two-dimensional shear flows. *J. Fluid Mech.* **78**, 385–413.
- ZHOU, H. & POZRIKIDIS, C. 1993*a* The flow of suspensions in channels: Single files of drops. *Phys. Fluids A* **5**, 311–324.
- ZHOU, H. & POZRIKIDIS, C. 1993*b* The flow of ordered and random suspensions of two-dimensional drops in a channel. *J. Fluid Mech.* **255**, 103–127.
- ZHOU, H. & POZRIKIDIS, C. 1994 Pressure-driven flow of suspensions of liquid drops. *Phys. Fluids* **6**, 80–94.